Clathrate hydrates in interstellar environment

Jyotirmoy Ghosh[a], Rabin Rajan J. Methikkalam[a,1], Radha Gobinda Bhuin[a,2], Gopi Ragupathy[a], Nilesh Choudhary[b], Rajnish Kumar[b,3], and Thalappil Pradeep[a,3]

[a]Department of Science and Technology (DST) Unit of Nanoscience and Thematic Unit of Excellence (TUE), Department of Chemistry, Indian Institute of Technology Madras, Chennai 600036, India; and [b]Department of Chemical Engineering, Indian Institute of Technology Madras, Chennai 600036, India

Edited by Francois Forget, Laboratoire de Météorologie Dynamique, Paris, France, and accepted by Editorial Board Member Jean Jouzel December 10, 2018 (received for review August 18, 2018)

Clathrate hydrates (CHs) are ubiquitous in earth under high-pressure conditions, but their existence in the interstellar medium (ISM) remains unknown. Here, we report experimental observations of the formation of methane and carbon dioxide hydrates in an environment analogous to ISM. Thermal treatment of solid methane and carbon dioxide–water mixture in ultrahigh vacuum of the order of 10^{-10} mbar for extended periods led to the formation of CHs at 30 and 10 K, respectively. High molecular mobility and H bonding play important roles in the entrapment of gases in the in situ formed 5^{12} CH cages. This finding implies that CHs can exist in extreme low-pressure environments present in the ISM. These hydrates in ISM, subjected to various chemical processes, may act as sources for relevant prebiotic molecules.

clathrate hydrate | interstellar medium | ISM | ultra-high vacuum | amorphous solid water

Clathrate hydrates (CHs) are crystalline inclusion compounds in which different guest molecules are encased in H-bonded water cages (1). These trapped molecules are generally small such as CH_4, CO_2, N_2, H_2, etc. Among several such known CHs, those of CH_4 and CO_2 have drawn close attention of the scientific community due to their use as potential future source of energy (1, 2) and in CO_2 sequestration (3), respectively. Natural methane and carbon dioxide hydrates are found in permafrost and marine sediments on the outer continental shelves (4) at ambient temperatures (<300 K) and moderately high pressures (6 atm) (1). They could also exist in many solar system bodies such as in the Martian permafrost (5–7), on the surface of Titan (8), and on other icy satellites due to the prevalent thermodynamic (high P, low T) conditions (9). The stabilizing conditions (generally high pressures) of methane hydrate suggest that it is nonexistent in ultrahigh vacuum (UHV). Near zero diffusion prevents molecular rearrangements at cryogenic conditions, making the formation of cage structures impossible for water at interstellar temperatures. Therefore, it is not surprising that there is no report of its existence in conditions of relevance to space. Using thermodynamic data of methane hydrate available in the literature, its stability was extrapolated to low T, P region as shown (*SI Appendix*, Fig. S1), which suggests stability up to 2×10^{-6} mbar at 30 K. This temperature and pressure range is very close to nebular pressures, which could reach as high as 10^{-3} mbar, and the temperature range can vary from 4 to 100 K (9). Equilibrium condensation curve of methane hydrate in protostellar nebula also suggests its stability $\sim 1 \times 10^{-8}$ mbar at 45 K (10).

Experimentally, in situ formation of CHs in UHV, and cryogenic interstellar conditions has not been explored. However, it was proposed that at low pressure, CH may be grown epitaxially on other preformed CHs or by annealing the condensed gas–water mixture (11). CH of CO_2 was obtained in a vacuum of 10^{-6} torr, but at 120 K (12). We have adopted the annealing method to obtain CHs. In experiments conducted in the temperature window of 10–160 K and at 10^{-10} mbar pressure, we observed CH_4 and CO_2 hydrates at temperatures near 30 and 10 K, respectively. Molecular mobility and structural rearrangement observed in these experiments at cryogenic conditions suggest unusual processes in water. The anomalous eruption of CH_4, CO_2, or other volatile gases in cold interstellar clouds or in comets could possibly be explained by the existence of such hydrates in gas-forming regions of the interstellar space (10, 12). Irradiation or annealing leads to the chemical evolution of ice in ISM, forming new species (13). CHs could be one such new chemical system in the ISM, which may be subjected to additional processing.

Results and Discussion

Fig. 1*A* displays time-dependent reflection absorption infrared (RAIR) spectra of 300 monolayers (MLs; 1 monolayer is equivalent to $\sim 1.0 \times 10^{15}$ molecules $\cdot$ cm^{-2}) of a codeposited mixture (1:1) of CH_4 and water at the C–H antisymmetric stretching region at three different temperatures (10, 20, and 30 K) and two different annealing times (0 and 25 h) under UHV. The annealing time is crucial for the success of the experiment. The figure clearly shows no change in peak position for the C–H antisymmetric stretching band of solid CH_4 (3,009 cm^{-1}) with time, at 10 and 20 K. This peak is due to the untrapped CH_4; in other words, CH_4 hydrate was not observed at 10 and 20 K. A completely new IR peak (3,017 cm^{-1}) appears alongside the peak at 3,009 cm^{-1} after 25 h of annealing at 30 K. This new peak (3,017 cm^{-1}) is attributed to the CH_4 hydrate, where CH_4 is trapped in the CH cage. The rest of the untrapped CH_4 remained in the pores of amorphous ice. The experimental blue shift of 8 cm^{-1} is due to the entrapment of CH_4 in the hydrate cage. Here, the trapped CH_4 inside the CH cage behaves more

Significance

Formation of clathrate hydrate (CH) requires high pressures and moderate temperatures, which enable their existence in marine sediments and the permafrost region of earth. The presence of CHs in interstellar medium (ISM) is still in question due to the extreme high vacuum and ultracold conditions present there. Here, we conclusively identified methane and carbon dioxide hydrates in conditions analogous to ISM. We found that molecular mobility and interactions play crucial roles in the formation of CHs, even though there is no external pressure to force cage formation. Various chemical processes on these hydrates in ISM may lead to relevant prebiotic molecules.

Author contributions: J.G. and T.P. designed research; J.G. and R.R.J.M. performed research; J.G., R.R.J.M., and T.P. contributed new reagents/analytic tools; J.G., R.R.J.M., R.G.B., G.R., N.C., R.K., and T.P. analyzed data; and J.G., R.R.J.M., R.G.B., G.R., R.K., and T.P. wrote the paper.

The authors declare no conflict of interest.

This article is a PNAS Direct Submission. F.F. is a guest editor invited by the Editorial Board.

[1]Present address: Institute of Chemistry, The Hebrew University, Jerusalem 91904, Israel.

[2]Present address: Lehrstuhl für Physikalische Chemie II, Friedrich-Alexander-Universität Erlangen-Nürnberg, 91058 Erlangen, Germany.

[3]To whom correspondence may be addressed. Email: rajnish@iitm.ac.in or pradeep@iitm.ac.in.

This article contains supporting information online at www.pnas.org/lookup/suppl/doi:10.1073/pnas.1814293116/-/DCSupplemental.

Published online January 10, 2019.

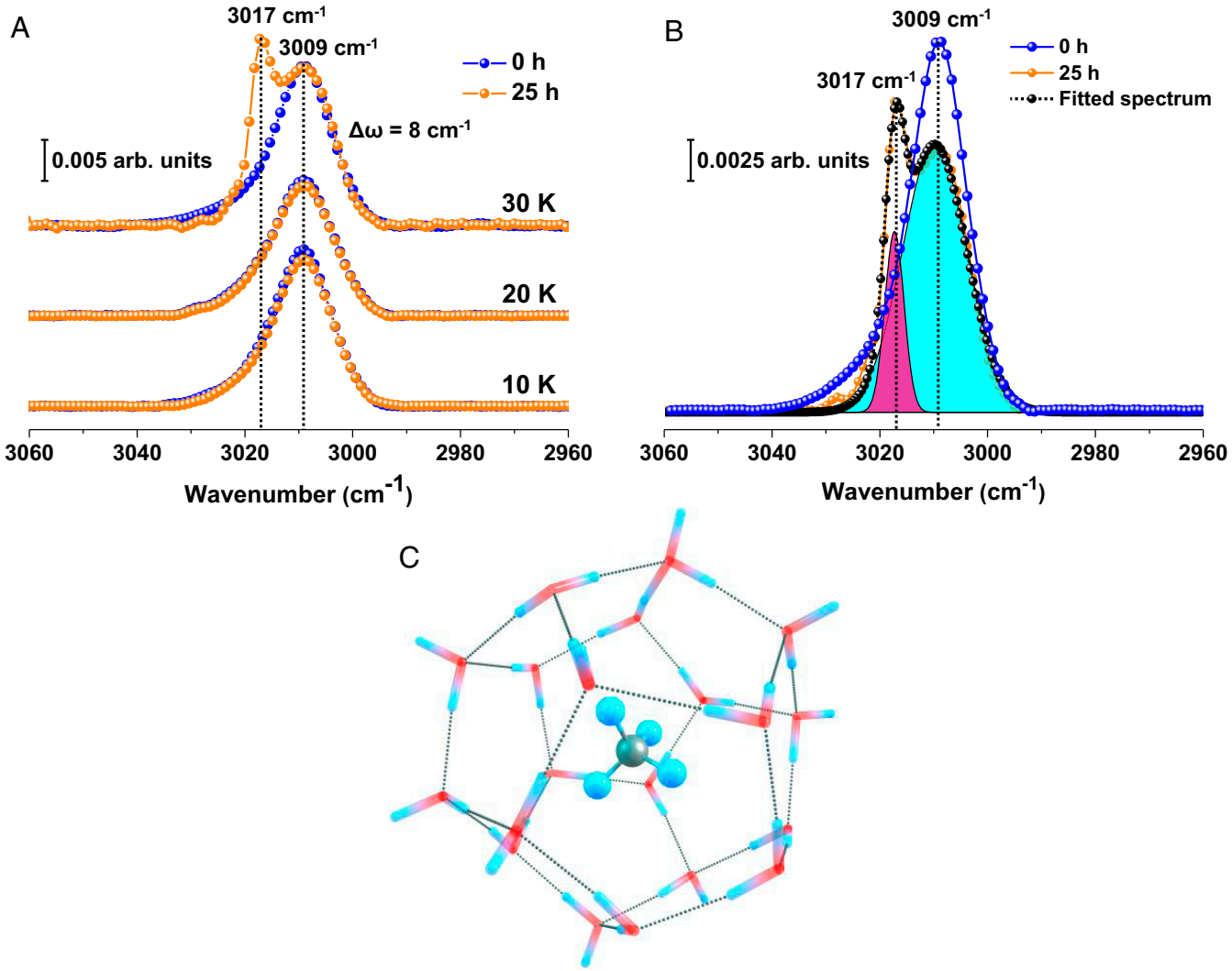

Fig. 1. CH_4 hydrate formation as studied by RAIR spectroscopy and quantum chemical calculations. (*A*) Normalized time-dependent RAIR spectra of 300 MLs CH_4+H_2O (1:1) mixed ice at 10, 20, and 30 K at the C–H antisymmetric stretching region. (*B*) Time-dependent RAIR spectra of the same system at 30 K. Here, the blue trace was divided by a factor of 7 to match the intensity of orange trace. Difference in intensity is due to desorption of CH_4 at 30 K, near its desorption temerature. Deconvoluted IR peaks are shown by cyan (3,009 cm^{-1}) and pink shade (3,017 cm^{-1}). (*C*) DFT-optimized structure of CH_4 trapped within CH (5^{12} cage). Here, water cage and guest molecule (CH_4) are shown. Color code used: gray, C; red, O; cyan, H.

like gaseous CH_4 as expected. It is known that vibrational frequency of free guest molecules in CH fall in between their vapor and condensed phase frequencies (14). The IR peak was deconvoluted to show the actual concentration of CH_4 trapped inside the hydrate cages and pores of amorphous solid water (ASW). The peak widths were calculated upon deconvolution, and the values were 14.1 and 4.2 cm^{-1} for the peaks at 3,009 and 3,017 cm^{-1}, respectively. Note the reduced width (4.2) of 3,017 cm^{-1} for the hydrate peak, characteristic of a unique structure. Taking the IR intensity, the extent of CH_4 in the hydrate form was estimated to be 12.71% of the total CH_4 at this condition. As the annealing temperature is close to that of desorption, about 6/7 of the adsorbed CH_4 desorbs during annealing. Furthermore, we confirmed the formation of CH_4 hydrate by quantum chemical calculations. Density functional theory (DFT) calculations of the CH_4 hydrate revealed that the small cage (5^{12}) as shown in Fig. 1*C* is favorable to form at this particular condition. Our computationally determined shift in the C–H antisymmetric mode during hydrate formation closely matches with the experimental value (*SI Appendix*, Table S1). A microsecond molecular dynamics simulation of CH_4 hydrate nucleation predicts preferential formation of smaller 5^{12} cages in the initial stages of CH_4 hydrate nucleation, supporting our observation (2).

Keeping the CH_4 and water ice mixture at 30 K for more than 25 h results in the formation of CH_4 hydrate. The long experimental time scale and the temperature (30 K), very near to the desorption temperature of CH_4, are two crucial factors for the formation of CH_4 hydrate under UHV conditions. We propose that prolonged subjugation of CH_4–water mixture at 30 K enhances the mobility of CH_4 molecules and leads to its insertion within the cages formed simultaneously. In a time-dependent study of 150 MLs of pure solid CH_4 at 25 K (*SI Appendix*, Fig. S2), the additional peak (3,017 cm^{-1}) was not observed. This is again a piece of evidence that the above peak is due to CH_4 hydrate.

To support our claim of the formation of CH in ISM, we have chosen a more stable hydrate, namely that of CO_2, which is already known to form CH at 120 K and 10^{-6} torr (12). Fig. 2*A* represents the temperature-dependent RAIR spectra of 300 MLs of the codeposited mixture (1:5 ratio) of CO_2 and water in the C = O antisymmetric stretching region. The figure shows two IR peaks for the C = O antisymmetric stretching band of solid CO_2 at 10 K. The peak at 2,353 cm^{-1} is attributed to the untrapped CO_2 that exists

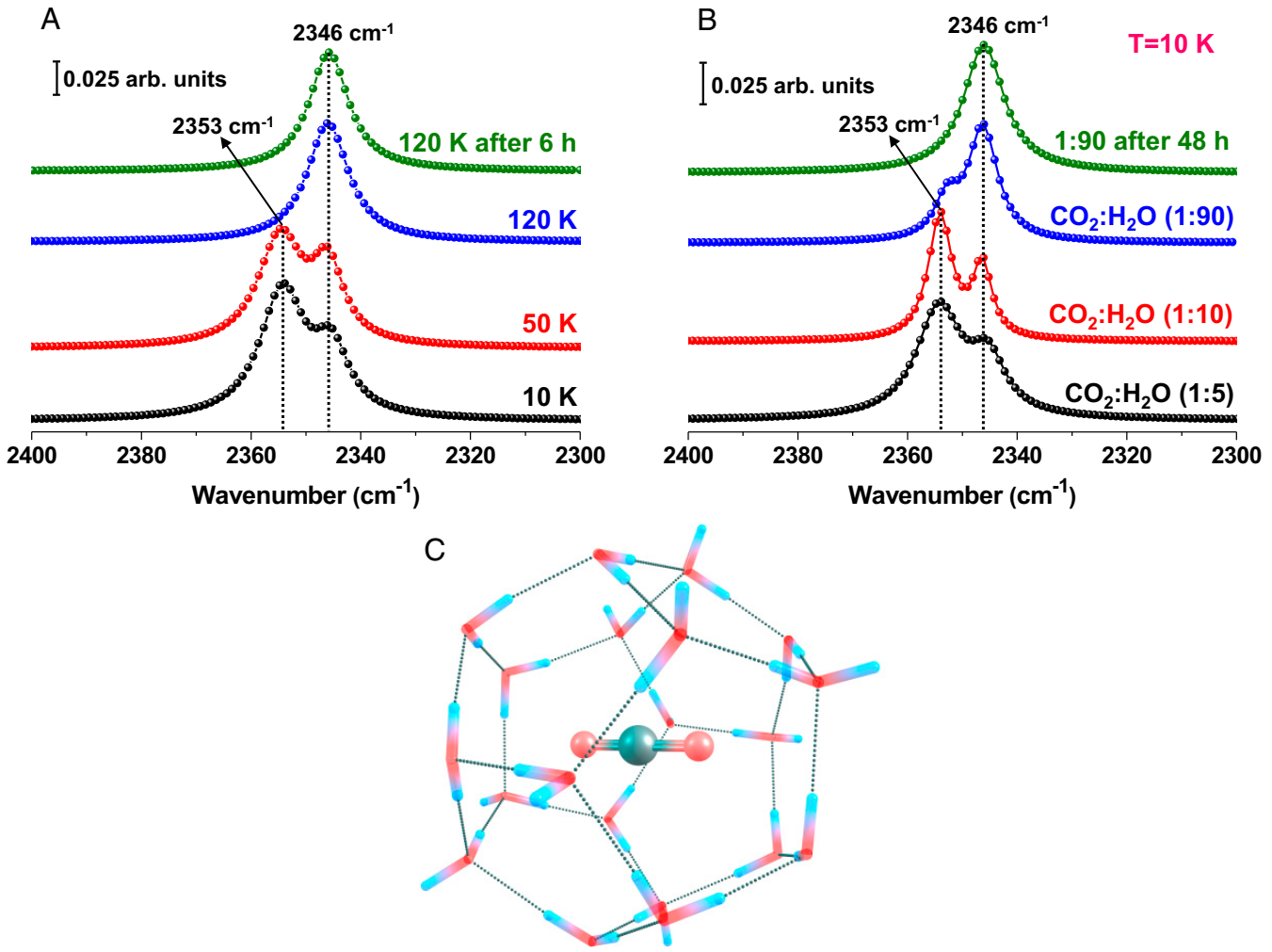

Fig. 2. CO_2 hydrate formation as studied by RAIR spectroscopy and quantum mechanical calculations. (*A*) Normalized temperature dependent RAIR spectra of 300 MLs CO_2+H_2O (1:5) mixed ice at C = O antisymmetric stretching region. A new peak at 2,346 cm^{-1} arises due to the formation of CO_2 hydrate. (*B*) Ratio-dependent RAIR spectra of 300 MLs CO_2+H_2O at 10 K (normalized). (*C*) DFT-optimized structure of CO_2 trapped inside CH (5^{12} cage). Here, water cage and guest molecule (CO_2) are shown. Color code used: gray, C; red, O; cyan, H.

outside of the CH cage, and in the amorphous pores of water ice. The other peak, positioned at 2,346 cm^{-1}, is due to the CO_2 entrapped in the CH cage (15, 16). Now, as the system was annealed further to 50 K (heating rate = 2 K · min^{-1}), the intensity of the CO_2 hydrate peak (2,346 cm^{-1}) increased and that of the free CO_2 peak (2,353 cm^{-1}) decreased. At 120 K, the untrapped CO_2 peak vanished completely and only the CO_2 hydrate peak remained. It indicates that the annealing of CO_2 mixed ice leads to the gradual formation of CO_2 hydrate and the transformation is complete at 120 K. Furthermore, no change in CO_2 hydrate peak position (2,346 cm^{-1}) was observed when the system was kept at 120 K for 6 h (Fig. 2*A*). This confirms that the CO_2 hydrate is quite stable in these analogous astrochemical conditions. It is also clear that CO_2 hydrate forms even at 10 K during deposition itself.

The stoichiometric ratio of water and guest molecules is an essential aspect of controlling the formation of CH (12). The ideal ratio of water and guest molecules is 20:1 for CH_3OH hydrate formed at 130 K and at 10^{-6} torr pressure (12). Fig. 2*B* shows the comparative formation of CO_2 hydrate at different ratios of CO_2:H_2O at 10 K under UHV. The figure clearly indicates that the intensity of 2,346 cm^{-1} peak is maximum for a 1:90 mixture compared with the other ratios. This suggests the optimum ratio needed for CO_2 hydrate formation at 10 K, which is a very diluted mixed ice. The shoulder at 2,353 cm^{-1} vanished upon keeping the ice at 10 K for over 48 h as shown in Fig. 2*B*, suggesting that all of the remaining free CO_2 forms hydrate structure over time.

We confirmed the formation of CO_2 hydrate by quantum chemical calculations. These calculations revealed that the small cage (5^{12}), as shown in Fig. 2*C*, is favorable to form. Our computationally determined shift in the C = O antisymmetric mode closely matches with the experimental vibrational shift upon hydrate formation. Here, CO_2 is interacting with the water cage through hydrogen bonding, and consequently, there is a red shift. This result agrees well with the experimental shift (*SI Appendix*, Table S1). Other possible cages computed ($5^{12}6^2$ and $5^{12}6^4$) have reduced or opposite shift, respectively (*SI Appendix*, Table S1). In *SI Appendix*, Table S2, we have presented the coordinates of optimized geometries of CH_4 and CO_2 in 5^{12}, $5^{12}6^2$, and $5^{12}6^4$ CH cages. In *SI Appendix*, Table S3, we have added the harmonic frequencies calculated for different cages of CH_4 CH and CO_2 CH.

The rapid formation of CO_2 hydrate compared with the slow kinetics seen for CH_4 hydrate is because of the induced polarity of CO_2. Nucleation mechanism of CH formation varies for different guest molecules and can depend on their chemical nature (17). During the nucleation of CO_2 hydrate structure, it interacts

with water through stronger interaction, whereas CH_4 is unable to interact similarly. We extended the analysis using Bader's theory of atoms in molecules (AIM) to confirm the nature of interaction of guest molecules with hydrate cages. The electron density $\rho(\mathbf{r_C})$ values obtained for the critical points between a particular atom of the guest species and the hydrate cage along with the corresponding Laplacian of the electron density ($\nabla^2\rho(\mathbf{r_C})$) are listed in *SI Appendix*, Table S4. The higher value of electron density ($\rho(\mathbf{r_C})$) for the critical point between the O atom of CO_2 and the hydrate cage (0.01563 a.u.) compared with that between the H atom of CH_4 (0.00598 a.u.) and the hydrate cage suggests that the interaction for CO_2 is stronger than that for methane.

In the previous experiments, codeposition of CO_2 and water results in CH. Sequential deposition was also carried out. Annealing of this sequentially deposited system, CO_2@H_2O (1:5 ratio), did not result in CO_2 hydrate and the 2,346 cm^{-1} peak was not observed (*SI Appendix*, Fig. S3). Here, the peak at 2,381 cm^{-1} is attributed to pure multilayer CO_2. This phenomenon strongly supports the fact that proper mixing of water and CO_2 is a crucial step for the formation of CO_2 hydrate. The codeposition method allows better mixing of CO_2 molecules with water, whereas sequential deposition does not. Sequential deposition of water over CO_2 may result in diffusional mixing, but this does not lead to the formation of CH.

About 1% of $^{13}CO_2$ is present along with $^{12}CO_2$ naturally as shown (*SI Appendix*, Fig. S4). During the $^{12}CO_2$ hydrate experiment, $^{13}CO_2$ also shows CH upon annealing to 120 K. Temperature-dependent RAIR spectra in the ^{13}C = O antisymmetric stretching region (*SI Appendix*, Fig. S5), where the 2,282 cm^{-1} peak is due to untrapped $^{13}CO_2$ and that at 2,278 cm^{-1} is due to $^{13}CO_2$ hydrate (15).

The formation of CHs in ISM condition is further confirmed by temperature programmed desorption-mass spectrometry (TPD-MS). The trapped guest molecules within ASW are released when amorphous to crystalline ice transition occurs at 140 K. Fig. 3*A* represents the comparative TPD spectra before and after the formation of CH_4 hydrate. The spectra correspond to CH_4 desorption and were monitored using the intensity of CH_3^+ alone. Peaks at 38 and 46 K correspond to multilayer CH_4 and CH_4 trapped in ASW (CH_4···ASW), respectively. These TPD peaks are assigned by a control study as shown (*SI Appendix*, Fig. S6). The CH_4 hydrate was formed by annealing a codeposited mixture at 30 K for 25 h, and during this course, most of the free CH_4 got desorbed, as observed from TPD. Desorption of CH_4 in trapped ASW got shifted to 53 K after the formation of CH. The abrupt release of trapped gases from ASW at 140 K is termed as

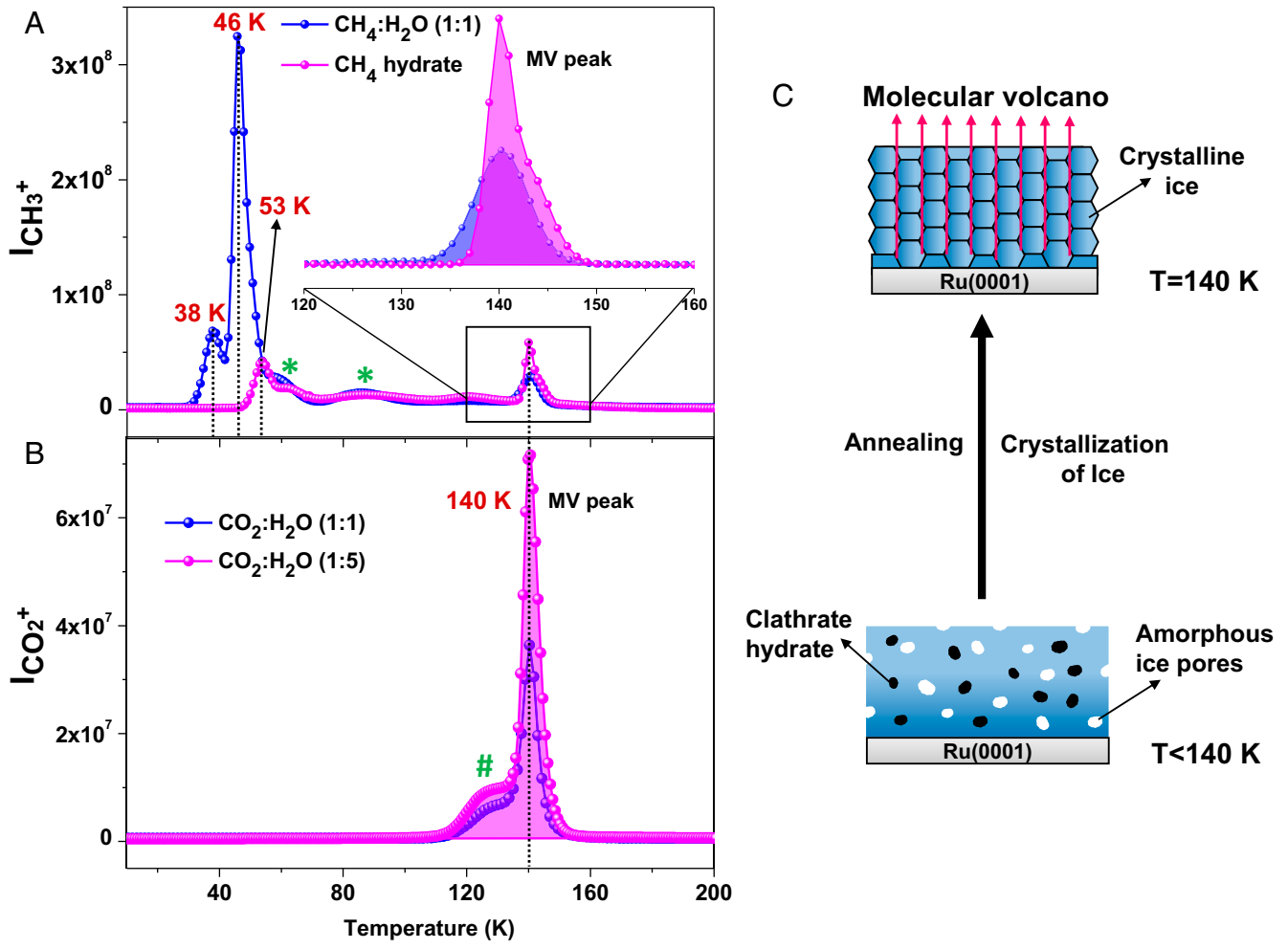

Fig. 3. TPD mass spectra of 300 MLs of codeposited ice systems at different ratio (heating rate = 30 K · min^{-1}). Here, the intensities of CH_3^+ (m/z = 15), and CO_2^+ (m/z = 44) are plotted. (*A*) Desorption of CH_4 after hydrate formation (magenta line) and before hydrate formation (blue line). MV peaks are shown in the *Insets*. *, peaks are attributed to desorption due to structural transitions of ASW upon annealing. (*B*) Desorption of CO_2 after hydrate formation at different ratios, as indicated. #, the peak is due to the predissociation of CO_2 hydrate cage. (*C*) Schematic representation of MV upon crystallization of ice.

molecular volcano (MV) (18, 19). The intensity of MV peak (at 140 K) increases, upon the formation of CH_4 hydrate. Before the formation of CH_4 hydrate, the MV peak is due to the trapped CH_4 in ASW. The reason for the enhancement of MV peak intensity is the simultaneous release of trapped CH_4 from ASW pores as well as from the CH_4 hydrate cage (Fig. 3*C*). Note that the amount of gases deposited is the same in both the cases. Slight distortion in the MV peak is attributed to the modification of ASW pores due to CH formation (Fig. 3*A*). The amount of desorption due to CH is estimated to be 14.53% of the total CH_4 at this condition, and it is correlated to the amount of CH calculated from the IR data (Fig. 1*B*).

In Fig. 3*B*, we compared the TPD spectra of 300 MLs of CO_2+H_2O at two ratios, 1:1 and 1:5, which were deposited at 10 K. Then, these two systems were annealed at 120 K for the complete formation of CO_2 hydrate. After that, they were cooled back to 10 K, and TPD mass spectra were taken. The heating rate for TPD was 30 K · min^{-1}. The peak at 140 K corresponds to MV of CO_2. Fig. 3*B* shows that the intensity of MV increased as the ratio of CO_2 and H_2O was changed from 1:1 to 1:5. Taking the area under the MV peaks, the amount of CH formed was found 1.7 times higher for (1:5) than the former. As previously explained, the extent of formation of CO_2 hydrate is greater for the latter ratio (Fig. 2). Here again, the enhancement agrees with the IR data. No additional desorption of CH_4 and CO_2 above this temperature suggest that the hydrates have been decomposed.

Conclusion

We have shown that CHs can form in UHV and they can exist in the ISM conditions down to 10 K and 10^{-10} mbar. The anomalous eruption of volatile gases in ISM could be explained by the existence of hydrates. Enclathration of these gases and additional processing (e.g., irradiation, heating, etc.) may result in complex organic or prebiotic molecules. We believe that the present report may have an impact on both astronomy and chemistry.

Materials and Methods

Experimental Setup. Experiments were conducted in an ultrahigh vacuum instrument (base pressure ~10^{-10} mbar), which was described elsewhere (20, 21). Briefly, the instrument consists of a UHV chamber made of stainless steel, equipped with RAIR spectroscopy and TPD mass spectrometry. The spectrometer can also perform low energy ion scattering and secondary ion mass spectrometry, which have not been used in the present work (20). Vacuum of the order of ~10^{-10} mbar is an essential condition for simulating the condition of ISM. Vacuum was maintained by three oil-free Turbo molecular pumps backed by diaphragm pumps (Pfeiffer Vacuum). The system has a collective pumping speed of ~400 L/s. The UHV system is fully covered with a heating jacket, which allows an easy bake out over the weekend. The pressure of the experimental chamber is monitored by a Bayard-Alpert gauge (Pfeiffer Vacuum), controlled by a "MaxiGauge" vacuum gauge controller (Pfeiffer, Model TPG 256 A).

A thin film of ice was grown on top of a Ru(0001) single crystal that was mounted on a copper holder, which in turn was attached at the tip of a closed cycle helium cryostat (Coldedge Technologies). The substrate temperature could be controlled from 8 to 1,000 K. Comprehensive heat shielding and excellent thermal contact between the substrate holder and the cryofinger allowed us to achieve 8 K in 2 h. For the present study, the temperature was measured by a thermocouple sensor attached to the substrate. Repeated heating to 300 K before vapor deposition ensured surface cleanliness, adequate for the present experiments. Temperature ramping was controlled and monitored by a temperature controller (Lakeshore 336) (20).

Sample Preparation. For the formation of methane hydrate, ~99.99% pure methane gas, purchased from Rana Industrial Gases & Products, was used. The gas lines were connected to the experimental chamber through a high-precision all-metal leak valve through which the flow rate or deposition pressure of different gases was controlled. These two deposition tubes or gas lines were directed to the center of the substrate. Out of the two sample inlet lines, one was used exclusively for methane or carbon dioxide while the other line was used exclusively for water vapor deposition. Here, Millipore water (H_2O of 18.2 MΩ resistivity), taken in a test tube, connected to the sample line through a glass-to-metal seal was used for the experiment. The Millipore water was further purified through several freeze–pump–thaw cycles before introduction into the UHV chamber. During the exposure of different samples into the UHV chamber, mass spectra were recorded with a residual gas analyzer (RGA) attached near to the sample inlet line. Recorded mass spectra were used as an indication of the purity of the samples as well as to measure the ratio of the mixtures. The ratio of the mixed ice was achieved by the proper adjustment of flow or inlet pressure of the sample gas by regulating the leak valves. The substrate was kept at a perpendicular position for the uniform growth of ice. Here, most of the experiments were performed using 300 MLs coverage of the mixed ice. One point to be noted is that all of the experiments were performed under multilayer deposition conditions, and therefore, the substrate does not play any significant role in the formation of CH. The deposition of molecular solids was controlled through leak valves, and ML coverage was calculated (18, 22) assuming that 1.33×10^{-6} mbar · s = 1 ML, which was estimated to contain ~1.1×10^{15} molecules · cm^{-2}. Surface coverages mentioned were quantitative by following a similar deposition method adopted elsewhere (23). The inlet pressure during the sample deposition was decided based on the coverage desired at the time of the experiment.

Typical Experimental Protocol. For the deposition of 300 MLs of 1:1 mixed methane and ice, the chamber was backfilled at a total pressure of ~5×10^{-7} mbar (where methane pressure was 2.5×10^{-7} mbar and water pressure was 2.5×10^{-7} mbar) and the mixture was exposed to the surface for 10 min. Evacuation of residual water from the experimental chamber is one of the most common issues with UHV experiments, particularly when we deposit large amounts of water. After deposition, we waited for a few minutes to reach the background pressure before starting the spectroscopic measurements. Periodic bake out of the chamber during weekends ensures the cleanliness of the chamber.

This 1:1 mixed methane and ice was slowly (heating rate = 2 K · min^{-1}) heated to 30 K, near the desorption temperature of methane. At this temperature, most of the methane sublimed, which was observed in the mass spectra recorded by the residual gas analyzer. After that, the remaining mixed ice was maintained at 30 K for over 25 h. The ice sample was constantly monitored by IR spectroscopy. In other words, time-dependent RAIRS were recorded over a period of 25 h. During such measurements, a few monolayers of additional water could be deposited but this is rather negligible to be reflected in the spectra. Variation of a few monolayers in coverage does not change the observed phenomena. During the time-dependent measurements, we maintained identical conditions from the beginning to the end. The position of the substrate, the external IR detector (mercury cadmium telluride; MCT), and the environment (dry N_2) in the IR spectrometer were kept constant throughout the experiment. A similar time-dependent RAIR study was carried out at 10 and 20 K also, and the spectra were collected for over 25 h as a separate set of experiments. IR exposure over extended periods did not have an effect on CH formation as revealed by studies at lower temperatures.

For the CO_2 hydrate study, 300 MLs of mixed ice was made by the codeposition of a mixture of CO_2:H_2O at 10 K. Different ratios (1:5, 1:10, and 1:90) of CO_2:H_2O were used. For each of the ratios, the total inlet pressure was kept at ~5×10^{-7} mbar, whereas the inlet pressures of CO_2 and water were varied according to the desired ratio. For the temperature-dependent measurements, after deposition of 1:5 ratio of CO_2:H_2O at 10 K, the sample was slowly heated (heating rate = 2 K · min^{-1}) up to 160 K. In another set of experiments, sequential deposition of CO_2 and water was carried out, where at first 150 MLs of CO_2 were deposited, which was followed by the deposition of 150 MLs of water at 10 K. By this way, we generated a sequentially deposited (CO_2@H_2O) film of equal coverage. A similar temperature-dependent IR study was carried out as described before, with this sequentially deposited film to observe the formation of CO_2 CH.

RAIRS Setup. RAIR spectra were recorded using a Bruker FT-IR spectrometer, Vertex 70. The external IR beam was focused onto the substrate using gold-plated mirrors through ZnSe windows (transparent to IR beam), attached to the vacuum chamber. The reflected IR beam from the substrate was refocused using another gold-plated mirror to a liquid N_2 cooled external MCT IR detector. The spectra were collected in the 4,000–550 cm^{-1} range with 2 cm^{-1} resolution. Each spectrum was an average of 512 scans to get a better signal-to-noise ratio. The IR beam path outside the UHV chamber was purged with dry N_2.

TPD-MS Setup. The clathrate hydrates were further characterized by TPD-MS analysis. For this, after ice deposition or clathrate hydrate formation (by following the method described earlier), the substrate was moved to a fixed position by using the sample manipulator to ensure that the surface is close to the mass spectrometer inlet. During TPD-MS measurements, the substrate was heated at a constant heating rate (30 $K \cdot min^{-1}$). Suitable mass of the desorbed species was selected by the RGA and the intensity of the desorbed species was plotted as a function of substrate temperature. Mass spectrometers were supplied by Extrel CMS (20). For TPD, the inlet of the mass spectrometer was positioned 50 mm from the center of the Ru substrate.

Computational Details. We examined the stability of clathrate hydrate cages and their CO_2, CH_4 inclusion complexes computationally. All of the considered cages of clathrate hydrates have been fully optimized at the B3LYP/6–311++G (d, p) level of theory using the Gaussian 09 program package (24). Frequency calculations characterize the obtained stationary points as minima on the potential energy surface. We sequentially added CO_2 and CH_4 molecules in 5^{12}, $5^{12}6^2$, and $5^{12}6^4$ clathrate hydrate cages and probed their cage occupancy. In general, the optimizations of clathrate hydrate cages were found to be quite challenging with the Gaussian programs. Normally, most optimizations of clathrate cages take a large number of steps and it was difficult to reach convergence. The B3LYP/6–311++G (d, p) level of theory was found to be reasonable for optimizations of clathrate hydrates and various other water clusters (14). The quantum theory of atoms in molecules methodology (25) was capable of revealing bonding interactions between individual functional groups and atoms in a molecule by the electron density distribution analysis.

All possible cages were considered in the present study. It was found that the 5^{12} clathrate hydrate cage was more stable; stability also depended on the size of the guest molecule. These results were also compared with the computational studies reported (14).

ACKNOWLEDGMENTS. J.G. thanks the University Grants Commission (UGC) for his research fellowship. We thank the Department of Science and Technology, Government of India, for supporting our research.

1. Sloan ED, Jr (2003) Fundamental principles and applications of natural gas hydrates. *Nature* 426:353–363.
2. Walsh MR, Koh CA, Sloan ED, Sum AK, Wu DT (2009) Microsecond simulations of spontaneous methane hydrate nucleation and growth. *Science* 326:1095–1098.
3. Park Y, et al. (2006) Sequestering carbon dioxide into complex structures of naturally occurring gas hydrates. *Proc Natl Acad Sci USA* 103:12690–12694.
4. Boswell R (2009) Engineering. Is gas hydrate energy within reach? *Science* 325: 957–958.
5. Chastain BK, Chevrier V (2007) Methane clathrate hydrates as a potential source for martian atmospheric methane. *Planet Space Sci* 55:1246–1256.
6. Swindle TD, Thomas C, Mousis O, Lunine JI, Picaud S (2009) Incorporation of argon, krypton and xenon into clathrates on Mars. *Icarus* 203:66–70.
7. Thomas C, Mousis O, Picaud S, Ballenegger V (2009) Variability of the methane trapping in martian subsurface clathrate hydrates. *Planet Space Sci* 57:42–47.
8. Tobie G, Lunine JI, Sotin C (2006) Episodic outgassing as the origin of atmospheric methane on Titan. *Nature* 440:61–64.
9. Mousis O, Lunine JI, Picaud S, Cordier D (2010) Volatile inventories in clathrate hydrates formed in the primordial nebula. *Faraday Discuss* 147:509–525, 527–552.
10. Luspay-Kuti A, et al. (2016) The presence of clathrates in comet 67P/Churyumov-Gerasimenko. *Sci Adv* 2:e1501781.
11. Mao WL, et al. (2002) Hydrogen clusters in clathrate hydrate. *Science* 297:2247–2249.
12. Blake D, Allamandola L, Sandford S, Hudgins D, Freund F (1991) Clathrate hydrate formation in amorphous cometary ice analogs in vacuo. *Science* 254:548–551.
13. Allamandola LJ, Bernstein MP, Sandford SA, Walker RL (1999) Evolution of interstellar ices. *Space Sci Rev* 90:219–232.
14. Buch V, et al. (2009) Clathrate hydrates with hydrogen-bonding guests. *Phys Chem Chem Phys* 11:10245–10265.
15. Fleyfel F, Devlin JP (1991) Carbon dioxide clathrate hydrate epitaxial growth: Spectroscopic evidence for formation of the simple type-II carbon dioxide hydrate. *J Phys Chem* 95:3811–3815.
16. Kumar R, Lang S, Englezos P, Ripmeester J (2009) Application of the ATR-IR spectroscopic technique to the characterization of hydrates formed by $CO_{(2)}$, $CO_{(2)}/H_{(2)}$ and $CO_{(2)}/H_{(2)}/C_{(3)}H_{(8)}$. *J Phys Chem A* 113:6308–6313.
17. Warrier P, Khan MN, Srivastava V, Maupin CM, Koh CA (2016) Overview: Nucleation of clathrate hydrates. *J Chem Phys* 145:211705.
18. Ghosh J, Hariharan AK, Bhuin RG, Methikkalam RRJ, Pradeep T (2018) Propane and propane-water interactions: A study at cryogenic temperatures. *Phys Chem Chem Phys* 20:1838–1847.
19. Smith RS, Petrik NG, Kimmel GA, Kay BD (2012) Thermal and nonthermal physiochemical processes in nanoscale films of amorphous solid water. *Acc Chem Res* 45: 33–42.
20. Bag S, et al. (2014) Development of ultralow energy (1-10 eV) ion scattering spectrometry coupled with reflection absorption infrared spectroscopy and temperature programmed desorption for the investigation of molecular solids. *Rev Sci Instrum* 85: 014103.
21. Bhuin RG, Methikkalam RRJ, Sivaraman B, Pradeep T (2015) Interaction of acetonitrile with water-ice: An infrared spectroscopic study. *J Phys Chem C* 119:11524–11532.
22. Eui-Seong M, Heon K, Yasuhiro O, Naoki W, Akira K (2010) Direct evidence for ammonium ion formation in ice through ultraviolet-induced acid-base reaction of NH_3 with H_3O^+. *Astrophys J* 713:906–911.
23. Kimmel GA, Petrik NG, Dohnálek Z, Kay BD (2005) Crystalline ice growth on PT(111): Observation of a hydrophobic water monolayer. *Phys Rev Lett* 95:166102.
24. Frisch MJ, et al. (2009) *Gaussian 09, Revision A.1* (Gaussian, Inc., Wallingford, CT).
25. Bader RFW (1990) *Atoms in Molecules. A Quantum Theory* (Oxford Univ Press, Oxford).